# KIS protects against adverse vascular remodeling by opposing stathmin-mediated VSMC migration in mice

Thomas H. Langenickel, Michelle Olive, Manfred Boehm,
Hong San, Martin F. Crook, and Elizabeth G. Nabel

Vascular Biology and Genomics Section, Genome Technology Branch, National Human Genome Research Institute, NIH, Bethesda, Maryland, USA.

**Vascular proliferative diseases are characterized by VSMC proliferation and migration. Kinase interacting with stathmin (KIS) targets 2 key regulators of cell proliferation and migration, the cyclin-dependent kinase inhibitor p27$^{Kip1}$ and the microtubule-destabilizing protein stathmin. Phosphorylation of p27$^{Kip1}$ by KIS leads to cell-cycle progression, whereas the target sequence and the physiological relevance of KIS-mediated stathmin phosphorylation in VSMCs are unknown. Here we demonstrated that vascular wound repair in $KIS^{-/-}$ mice resulted in accelerated formation of neointima, which is composed predominantly of VSMCs. Deletion of $KIS$ increased VSMC migratory activity and cytoplasmic tubulin destabilizing activity, but abolished VSMC proliferation through the delayed nuclear export and degradation of p27$^{Kip1}$. This promigratory phenotype resulted from increased stathmin protein levels, caused by a lack of KIS-mediated stathmin phosphorylation at serine 38 and diminished stathmin protein degradation. Downregulation of stathmin in $KIS^{-/-}$ VSMCs fully restored the phenotype, and stathmin-deficient mice demonstrated reduced lesion formation in response to vascular injury. These data suggest that KIS protects against excessive neointima formation by opposing stathmin-mediated VSMC migration and that VSMC migration represents a major mechanism of vascular wound repair, constituting a relevant target and mechanism for therapeutic interventions.**

## Introduction

Vascular remodeling and wound repair constitute complex mechanisms aimed at restoration of vessel integrity and vessel function. This involves cells within the vessel wall, predominantly VSMCs, and the recruitment of inflammatory cells to the lesion site (1). Cell proliferation and migration are the most important response mechanisms leading to repopulation of the vascular wound. Both processes are tightly controlled and regulated by the cyclin-dependent kinase (CDK) inhibitor p27$^{Kip1}$ and the microtubule destabilizing protein stathmin, which are connected by their common kinase, kinase interacting with stathmin (KIS).

KIS was first identified in a yeast 2-hybrid screen as an interacting partner of stathmin (2). We later identified KIS as an interacting partner of p27$^{Kip1}$ (3). KIS is expressed in all adult tissues, is located in the nucleus and cytoplasm, and possesses an N-terminal kinase domain and a C-terminal RNA recognition motif with high homology to the corresponding motif of the mammalian splicing factor U2AF$^{65}$ (4). Although the kinase domain contains dual serine/threonine kinase characteristic sequences, KIS preferentially targets proline directed serine residues (5).

p27$^{Kip1}$ belongs to the Cip/Kip family of CDK inhibitors. It binds cyclin E-Cdk2, leading to inactivation of the cyclin-CDK complex and G$_1$/S arrest (6, 7). p27$^{Kip1}$ regulates vascular remodeling by inhibiting VSMC proliferation and promoting mobilization of blood- and bone marrow–derived inflammatory cells (1). KIS phosphorylates p27$^{Kip1}$ at serine 10 during the G$_1$ phase of the
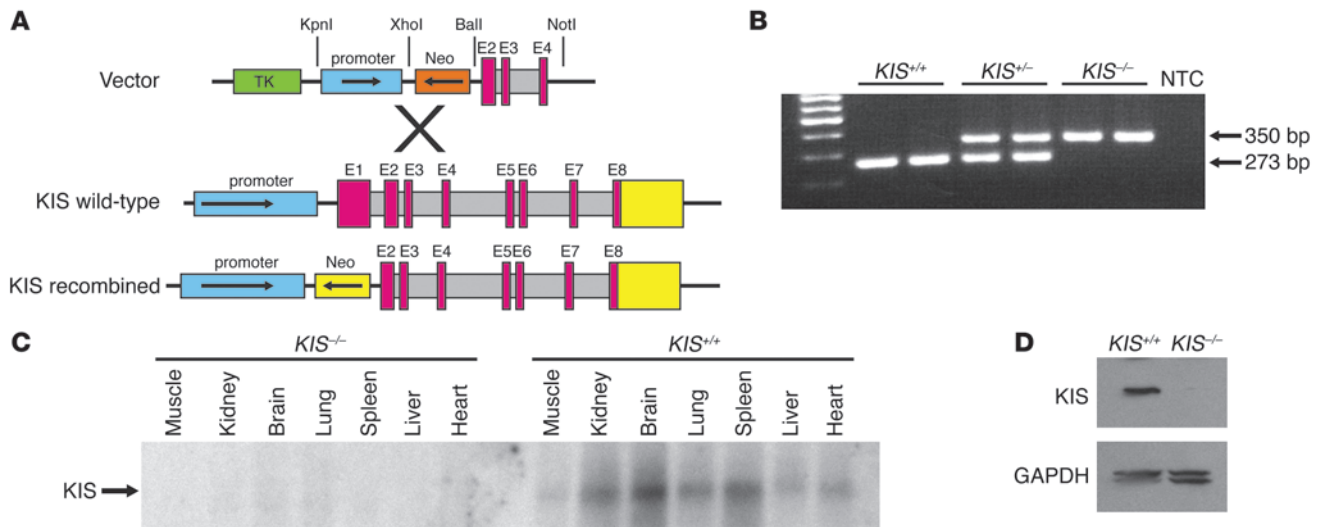
cell cycle in a mitogen-dependent manner, thereby causing nuclear export of p27$^{Kip1}$ and cell cycle progression (3).

Stathmin (encoded by $Stmn1$) is a small cytoplasmic phosphoprotein proposed to integrate diverse cellular signaling pathways. Several kinases target stathmin, including KIS, PKA, MAPK, CDK2, p34$^{cdc2}$, and CaM kinase II and IV (2). Stathmin complexes with $\alpha/\beta$ tubulin heterodimers and destabilizes tubulin by preventing assembly and forcing disassembly of microtubules (8, 9). The activity of stathmin is determined by phosphorylation on its 4 serine residues: 16, 25, 38, and 63 (10–12). Timely regulation of stathmin activity is important for accurate cell division. This is accomplished by deactivation of stathmin during spindle formation in the G$_2$/M phase of the cell cycle by p34$^{cdc2}$-dependent phosphorylation at serine 25 and 38. Forced expression of a p34$^{cdc2}$ target site–deficient mutant of stathmin led to G$_2$/M arrest (13–15). Moreover, stathmin has been proposed to promote cell migration. Mouse embryonic fibroblasts (MEFs) derived from $Stmn1^{-/-}$ mice displayed reduced migratory activity through fibronectin (16), and stathmin downregulation was correlated with low migratory activity of human sarcoma cells and impaired neuronal migration in rats (16, 17). $Stmn1^{-/-}$ mice did not display a developmental phenotype; however, in aging mice, stathmin was suggested to play an important role in maintenance of axonal integrity because they displayed central and peripheral axonal degeneration (18). Ablation of stathmin further led to memory deficits in innate and learned fear based on increased amount of microtubules and impaired induction of long-term potentials in the amygdala of the brain (19). These data provide in vivo evidence of the importance of stathmin in regulation of cell motility. Although KIS has been described as an interacting partner of stathmin in vitro, the phosphorylation sites targeted by KIS and the physiological impact of stathmin phosphorylation by KIS in vivo are unknown.

**Figure 1**
Generation of *KIS⁻/⁻* mice. (**A**) KIS was deleted by homologous recombination, replacing the kinase domain–encoding exon 1 with a neomycin resistance gene. (**B**) Representative PCR-based genotyping of wild-type *KIS⁺/⁺*, heterozygous *KIS⁺/⁻*, and homozygous *KIS⁻/⁻* mice. NTC, no template control. (**C**) Northern blot analysis confirmed absent KIS transcripts in tissues from *KIS⁻/⁻* mice. (**D**) KIS was not expressed in *KIS⁻/⁻* VSMCs, as revealed by Western blotting. GAPDH served as loading control.

In the present study, we demonstrate that deletion of KIS leads to accelerated neointima formation and vessel occlusion in an experimental mouse model of vascular wound repair. This phenotype resulted from increased migratory activity of VSMCs due to reduced KIS-dependent phosphorylation and diminished degradation of stathmin. Deletion of KIS also led to retained nuclear p27$^{Kip1}$, delayed cell cycle progression, and reduced growth rate of *KIS⁻/⁻* VSMCs. These data suggest that KIS protects from excessive vascular remodeling and further implicate KIS and stathmin as interesting therapeutic targets to modulate vascular remodeling processes involving cell migration.

## Results

*Generation of KIS⁻/⁻ mice.* *KIS⁻/⁻* mice were generated by homologous recombination targeting exon 1, which encodes for the kinase activity domain of KIS (Figure 1A). Mice were genotyped by Southern blot and PCR (Figure 1B), and lack of KIS expression was confirmed by Northern (Figure 1C) and Western blot (Figure 1D). Real-time PCR, using RNA isolated from *KIS⁺/⁺* and *KIS⁻/⁻* embryos, did not reveal full-length (primer spanning exon 1/2 boundary) or truncated KIS mRNA (primer spanning exon 3/4 and 7/8 boundaries) in *KIS⁻/⁻* embryos (data not shown). *KIS⁻/⁻* mice were viable and fertile and did not display organ abnormalities, including the vasculature (data not shown). No differences in body weight (*KIS⁺/⁺* male, $27.44 \pm 0.63$ g, $n = 8$; *KIS⁺/⁺* female, $22.82 \pm 0.80$ g, $n = 6$; *KIS⁻/⁻* male, $26.80 \pm 0.49$ g, $n = 8$; *KIS⁻/⁻* female, $21.88 \pm 0.68$ g, $n = 5$) or plasma triglyceride levels (*KIS⁺/⁺*, $51.86 \pm 5.19$ mg/dl; *KIS⁻/⁻*, $67.71 \pm 12.05$ mg/dl; $n = 7$ per group) were present. Plasma cholesterol was elevated in *KIS⁻/⁻* mice (*KIS⁺/⁺*, $68.86 \pm 2.91$ mg/dl; *KIS⁻/⁻*, $122.29 \pm 9.19$ mg/dl; $n = 7$ per group; $P < 0.01$) for unclear reasons; the short exposure to modest elevations did not appear to influence vascular remodeling, as lipid-rich lesions were not present (data not shown).

*Accelerated neointima formation in response to vascular injury in KIS⁻/⁻ mice.* To investigate the phenotype of vascular remodeling in *KIS⁻/⁻* mice, we performed femoral artery wire injury and measured neointima formation 7 and 14 days later. We observed an accelerated development of neointima in *KIS⁻/⁻* compared with *KIS⁺/⁺* mice, apparent at 7 days and progressive at 14 days after injury (intima/media area ratio, 7-day *KIS⁺/⁺*, $0.28 \pm 0.05$; 7-day *KIS⁻/⁻*, $0.63 \pm 0.10$; $P < 0.01$; 14-day *KIS⁺/⁺*, $0.49 \pm 0.15$; 14-day *KIS⁻/⁻*, $1.54 \pm 0.13$; $P < 0.001$; Figure 2, A and B).

We wondered whether this advanced lesion formation was attributable to cell proliferation, migration, or both mechanisms. To explore cell proliferation in vivo, we measured BrdU-labeled intimal and medial cells in femoral arteries harvested 1, 3, 5, 7, and 14 days after vascular injury (Figure 2C). Surprisingly, we did not observe a significant increase in cell proliferation within the intima or media of *KIS⁻/⁻* arteries compared with *KIS⁺/⁺* arteries at any time point (Figure 2D). The larger intimal lesions in the *KIS⁻/⁻* mice, in the absence of significant increases in proliferation, suggest that VSMC migration may play a role in vascular wound repair in these mice.

To further explore the role of cell migration, we analyzed the time course of VSMC appearance on the luminal surface of injured vessels using SMA immunoreactivity 1, 3, and 5 days after vascular injury. We observed an increased number of luminal VSMCs in *KIS⁻/⁻* mice, which was statistically significant 5 days after injury (Figure 3, A and B). These findings support the concept of increased VSMC migration in *KIS⁻/⁻* arteries because we did not observe an increase in cell proliferation within *KIS⁻/⁻* arteries at the same time points.

*Role of inflammation in KIS⁻/⁻ lesion formation.* Previous studies from our laboratory have suggested that inflammatory cells contribute to vascular lesion remodeling (1). To explore the role of inflammation, we investigated SMA-negative cells within *KIS⁻/⁻* lesions by immunostaining to detect T cells (CD3), macrophages (F4/80), and neutrophils. T cells (Figure 4A) were abundant in the intima and adventitia of *KIS⁻/⁻* arteries compared with *KIS⁺/⁺* controls, whereas we observed no difference in macrophage recruitment (Figure 4B). Neutrophils were not present in injured vessels of either genotype (data not shown).
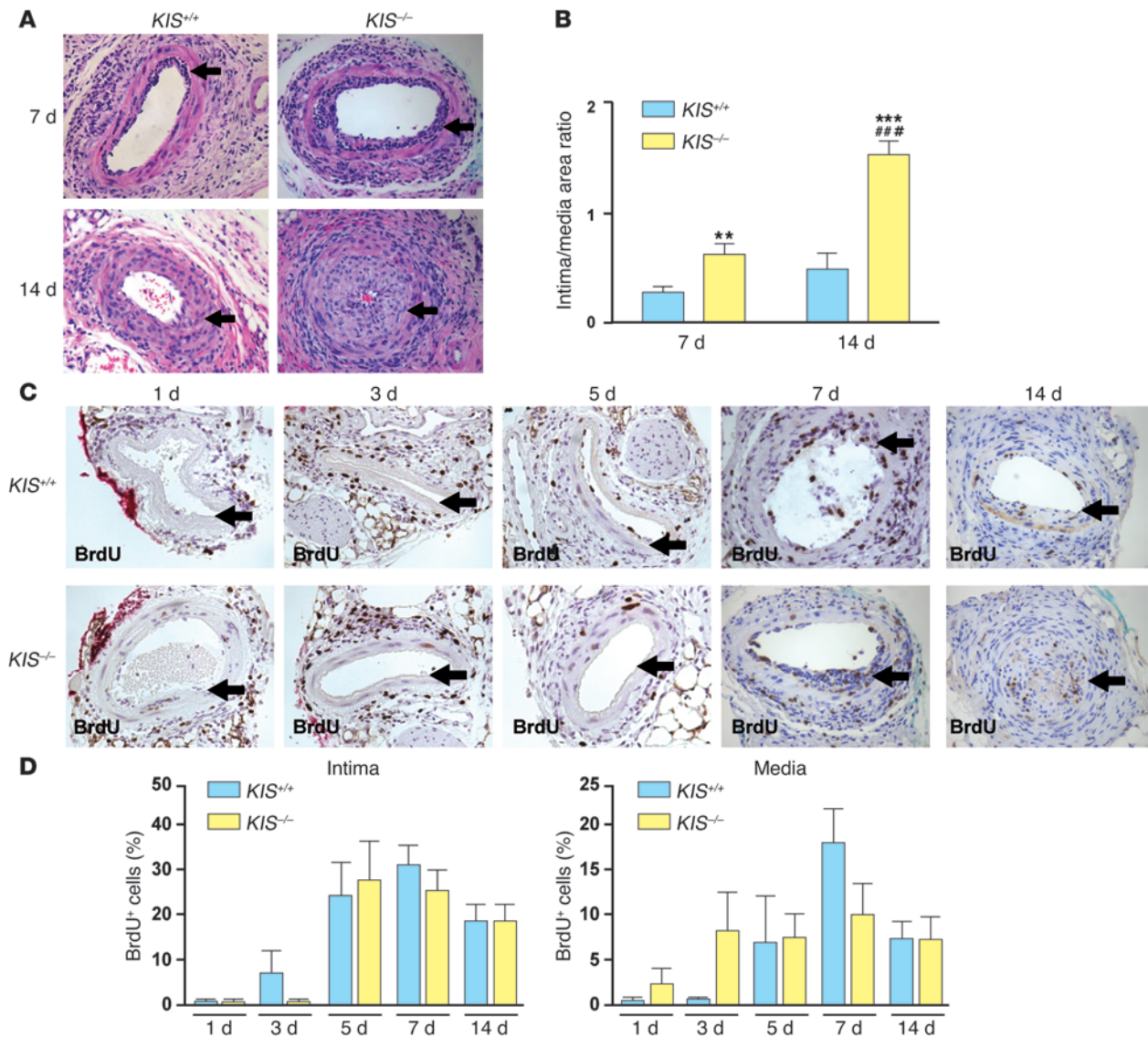
**Figure 2**
KIS protects from excessive neointima formation upon wire injury of the mouse femoral artery. (**A**) Representative H&E-stained sections of femoral arteries 7 and 14 days after wire injury in $KIS^{+/+}$ and $KIS^{-/-}$ mice. Arrows denote internal elastica. (**B**) Quantitative analysis of intimal hyperplasia, measured as intima/media area ratios, at 7 and 14 days. $n = 10$ mice per group. (**C** and **D**) BrdU immunostaining (**C**) and quantification of BrdU staining (**D**) did not show any differences in the number of intimal or medial BrdU$^+$ cells in $KIS^{+/+}$ and $KIS^{-/-}$ mice during the full time course of the experiment. Arrows denote internal elastica. $n = 5$–15 vessels per group (intima and media). Original magnification, ×400. $**P < 0.01$, $***P < 0.001$ vs. $KIS^{+/+}$; $^{\#\#\#}P < 0.001$ versus 7-day $KIS^{-/-}$.

To elucidate the role of T cells in the process of neointima formation, we crossbred $KIS^{-/-}$ mice with $Rag^{-/-}$ mice, which lack T and B cells, and performed vascular injury experiments. We observed no difference in the extent of neointima formation between $KIS^{-/-}$ $Rag^{+/+}$ and $KIS^{-/-}Rag^{-/-}$ arteries 14 days after vascular injury (Figure 4, C and D), which suggests that T and B cells do not markedly enhance the accelerated neointima formation observed in $KIS^{-/-}$ mice in this experimental model.

*Delayed cell cycle progression of $KIS^{-/-}$ VSMCs.* The major targets of KIS are p27$^{Kip1}$ and stathmin. We hypothesized that the lack of increased proliferation in $KIS^{-/-}$ VSMCs in vivo may result from disruption of p27$^{Kip1}$ and/or stathmin signaling. Accordingly, we

first investigated the effects of p27$^{Kip1}$ on cell cycle progression and cell proliferation in $KIS^{-/-}$ VSMCs in vitro. $KIS^{+/+}$ and $KIS^{-/-}$ VSMCs were serum starved for 72 hours, followed by release into the cell cycle by stimulation with 20% serum-containing medium. Degradation of p27$^{Kip1}$ measured in the total cellular protein fraction 12 hours after release into the cell cycle was reduced in $KIS^{-/-}$ versus $KIS^{+/+}$ VSMCs (Figure 5A). Furthermore, we observed substantial nuclear retention of p27$^{Kip1}$ protein 8 hours after release in $KIS^{-/-}$ versus $KIS^{+/+}$ VSMCs (Figure 5B), resulting in reduced BrdU incorporation and delayed S-phase entry 24 hours after release (Figure 5C) and reduced growth rate of $KIS^{-/-}$ VSMCs (Figure 5D). Interestingly, we observed p27$^{Kip1}$ localization in the nucleus of
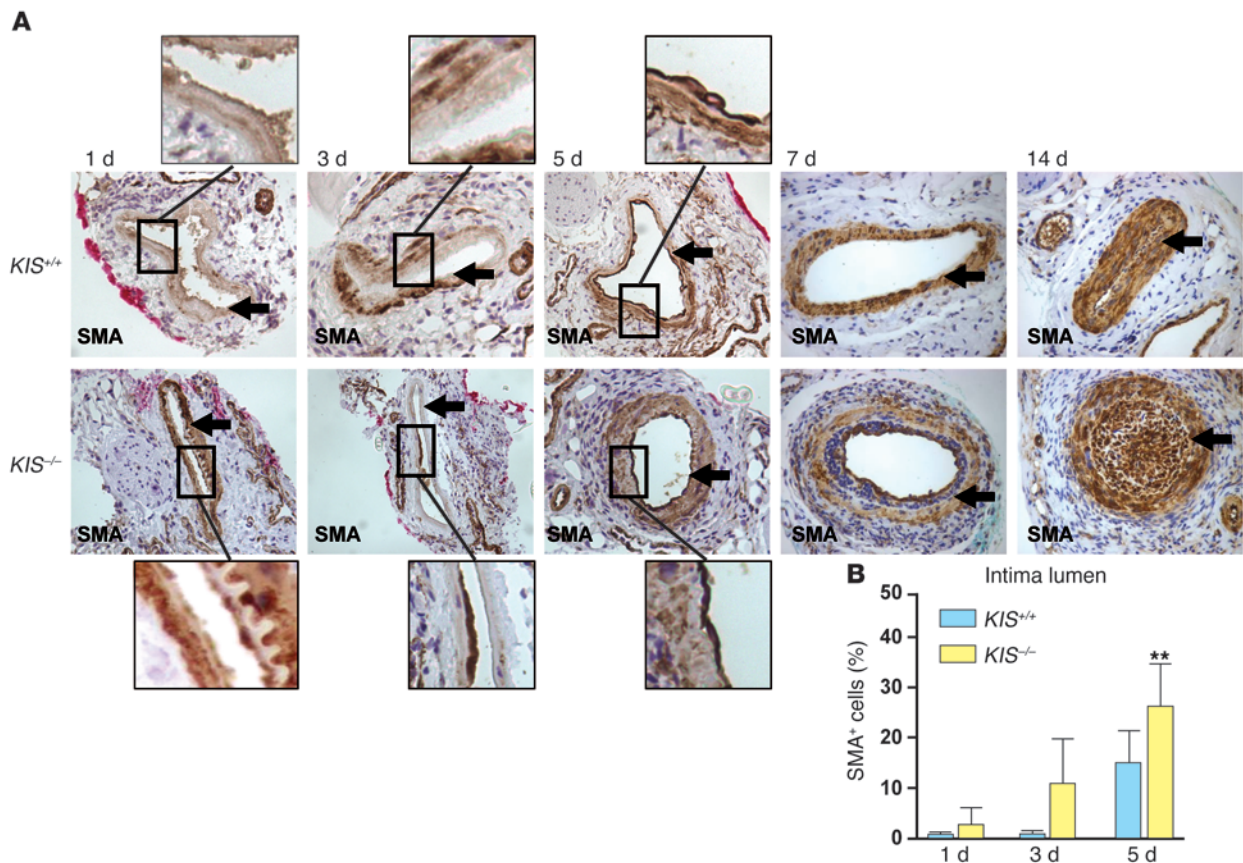
**Figure 3**
KIS inhibits migration of VSMCs into vascular lesions after wire injury of the mouse femoral artery. (**A**) SMA staining demonstrated increased recruitment of VSMCs into lesions in *KIS*^{−/−} mice. Arrows denote internal elastica. SMA^{+} cells appeared earlier on the luminal surface of the injured vessels in *KIS*^{−/−} than in *KIS*^{+/+} mice (insets). Original magnification, ×400; ×1,120 (insets). (**B**) Quantification revealed significantly more luminal SMA^{+} cells 5 days after vascular injury in *KIS*^{−/−} mice. *n* = 5–10 vessels per group. **$P < 0.01$ vs. *KIS*^{+/+}.

resting, serum-starved VSMCs in both genotypes; however, 8 hours after release into the cell cycle, p27[Kip1] was significantly retained in the nuclei of *KIS*^{−/−} compared with *KIS*^{+/+} VSMCs (Figure 5E), measured by quantification of p27[Kip1] immunostaining (Figure 5F). Taken together, these data suggest that KIS deletion leads to delayed p27[Kip1] nuclear export and cell cycle progression, resulting in reduced growth rates of *KIS*^{−/−} VSMCs.

*Increased migratory activity of KIS^{−/−} VSMCs and MEFs.* Because we did not observe an increase in proliferation of *KIS*^{−/−} VSMCs that would account for the accelerated neointima formation in *KIS*^{−/−} mice in vivo, we next investigated migratory properties of VSMCs and MEFs derived from *KIS*^{−/−} and *KIS*^{+/+} mice. Cell migration was assessed using a transwell system allowing for cell migration through 8-μm pores toward a serum gradient and PDGF-BB. *KIS*^{−/−} VSMCs (Figure 6A) and MEFs (Figure 6B) migrated significantly faster than did *KIS*^{+/+} cells over a period of 2 hours. We confirmed these findings using a fluorescence-based assay that permits real-time assessment of cell migration, in which we observed increased migratory activity of *KIS*^{−/−} VSMCs over 500 minutes (Figure 6, C and D).

We next measured VSMC adherence to fibronectin, as interaction between VSMCs and the extracellular matrix is important to promote cell migration, and fibronectin was used as matrix in the migration assays. We observed no differences in VSMC attachment to fibronectin over 30 minutes between *KIS*^{−/−} and *KIS*^{+/+} VSMCs (Figure 6E), excluding the possibility that the results of the in vitro migration assays resulted from altered VSMC adherence to fibronectin. These data suggest that increased VSMC migration within vascular lesions constitutes a mechanism accounting for accelerated neointima formation in *KIS*^{−/−} mice.

*Stathmin protein expression is upregulated in KIS^{−/−} VSMCs.* Given the increased migratory activity of *KIS*^{−/−} VSMCs, we investigated the expression and function of stathmin, a cytoplasmic target of KIS that has previously been shown to promote cell migration in cell types other than VSMCs (16, 20). Stathmin protein levels were increased about 3-fold in serum-starved *KIS*^{−/−} compared with *KIS*^{+/+} VSMCs (Figure 7, A and B). This difference was even more pronounced in VSMCs that had been serum stimulated for 12 or 24 hours (Figure 7, A and B). Given that the activity of KIS is regulated in a mitogen-dependent manner, these data suggest that KIS regulates degradation of stathmin by phosphorylation, and therefore a lack of KIS leads to increased stathmin protein abundance in *KIS*^{−/−} VSMCs. This hypothesis was confirmed in vivo by stathmin immunostaining of injured vessels, demonstrating increased stathmin immunoreactivity within the media and neointima of *KIS*^{−/−} mice 7 and 14 days after vascular injury (Figure 7C). Furthermore,
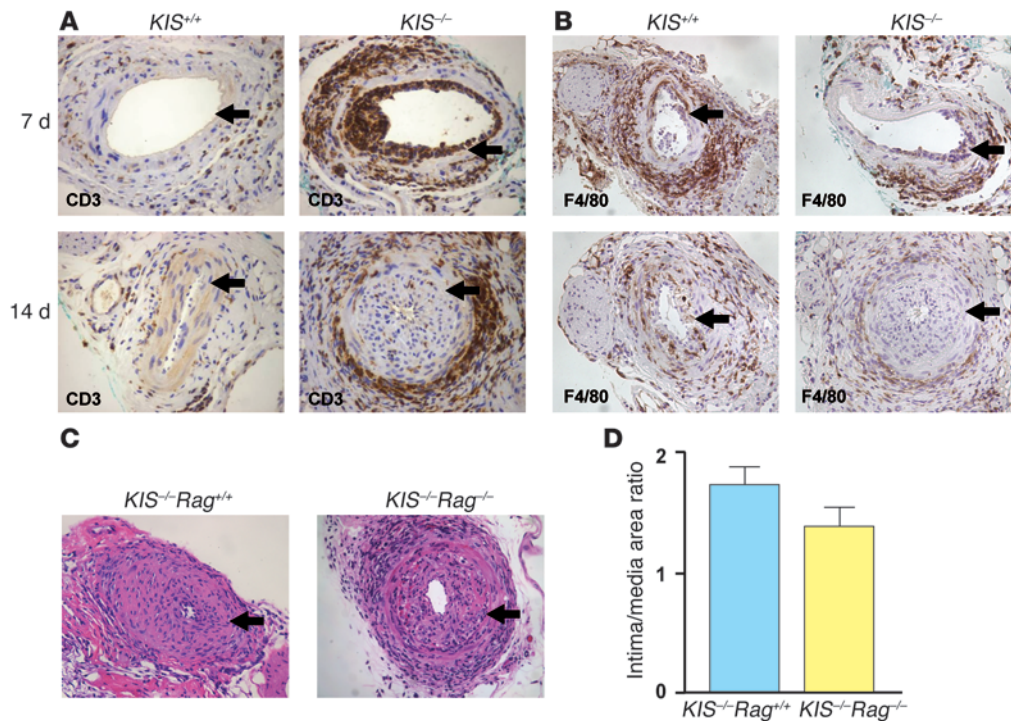
**Figure 4**
Role of inflammation in *KIS*⁻/⁻ lesion formation. (**A**) Immunohistochemistry demonstrated increased recruitment of T cells (CD3⁺) to the site of lesion in *KIS*⁻/⁻ mice, predominantly located to neointima (7 days after injury) and adventitia (7 and 14 days after injury). Arrows denote internal elastica. (**B**) Immunohistochemistry demonstrated no marked difference in macrophage (F4/80⁺) recruitment to the site of lesions between *KIS*⁺/⁺ and *KIS*⁻/⁻ mice. Arrows denote internal elastica. (**C** and **D**) *KIS*⁻/⁻*Rag*⁻/⁻ mice demonstrated the same excessive neointima formation as did *KIS*⁻/⁻*Rag*⁺/⁺ mice, demonstrated by representative H&E-stained sections (**C**; arrows denote internal elastica) and quantification of intima/media area ratios (**D**; *P* = NS; *n* = 5–8 vessels per group). Original magnification, ×400.

p27^Kip1 immunoreactivity was also significantly increased in *KIS*⁻/⁻ medial and intimal cells 7 and 14 days after vascular injury (Figure 7D). The increased p27^Kip1 immunoreactivity in *KIS*⁻/⁻ vessels is consistent with our findings from Western blot and immunostaining experiments presented earlier (Figure 5, A, B, E, and F) and are likely the result of reduced p27^Kip1 degradation caused by KIS deficiency.

In addition, we observed an increase in glycosaminoglycans in *KIS*⁻/⁻ arteries 14 days after injury compared with *KIS*⁺/⁺ arteries (Figure 7E), which suggests that extracellular matrix accumulation can contribute to the increased neointimal thickening in *KIS*⁻/⁻ arteries. This extracellular matrix is likely a product of accumulated VSMCs that undergo a phenotypic switch from contractile to synthetic state, but may also participate in the stathmin-triggered increase in *KIS*⁻/⁻ VSMC migration.

*KIS promotes stathmin degradation by phosphorylation at serine 38.* To confirm that stathmin degradation is impaired in *KIS*⁻/⁻ VSMCs, we measured stathmin protein expression in VSMCs that were serum starved for 72 hours and in VSMCs that were released into the cell cycle by serum stimulation for 12 hours in the absence or presence of the proteasome inhibitor β-clasto lactacystin (LC). Stathmin was degraded upon release of serum-starved *KIS*⁺/⁺ VSMCs into the cell cycle, whereas this cell cycle–dependent degradation was absent in *KIS*⁻/⁻ VSMCs (Figure 8A). Cell cycle–dependent degradation of stathmin was inhibited by LC in *KIS*⁺/⁺ VSMCs, whereas LC had no effect on stathmin expression in released *KIS*⁻/⁻ VSMCs (Figure 8A), which suggests that the

observed differences in protein abundance were the consequence of impaired degradation of stathmin in *KIS*⁻/⁻ VSMCs.

The most likely mechanism by which KIS regulates stathmin degradation is phosphorylation. In fact, KIS interacts and phosphorylates stathmin in vitro; however, the phosphorylation sites targeted by KIS and the functional consequences of this phosphorylation are not known. We therefore performed in vitro kinase assays using recombinant stathmin or phosphorylation site mutants of stathmin as substrates and KIS as kinase. Because KIS predominantly phosphorylates proline-directed serine residues, 2 serines (position 25 and 38), both within an SP motif of stathmin, were mutated to alanine. Although KIS phosphorylated stathmin, phosphorylation of S38A and S25/38A mutants was greatly reduced or not detectable (Figure 8B), which suggests that KIS targets serine 38. Phosphorylation of the S25A mutant was unaffected (Figure 8B). The additional band of higher molecular weight in the autoradiography of phosphorylated stathmin (Figure 8B) may result from unspecific phosphorylation of stathmin at multiple other sites, such as serines 16 and 63, by kinases other than KIS present in the immunoprecipitate. Both p34^cdc2, which is known to phosphorylate stathmin at serine 25 and 38, and PKA, which phosphorylates stathmin at serine 16 and 63, were used as controls. Whereas p34^cdc2 phosphorylated stathmin but not S25/38A mutated stathmin, PKA phosphorylated both forms as expected (Figure 8C). To further confirm the importance of serine 38 phosphorylation for stathmin degradation in vivo, we cotrans-
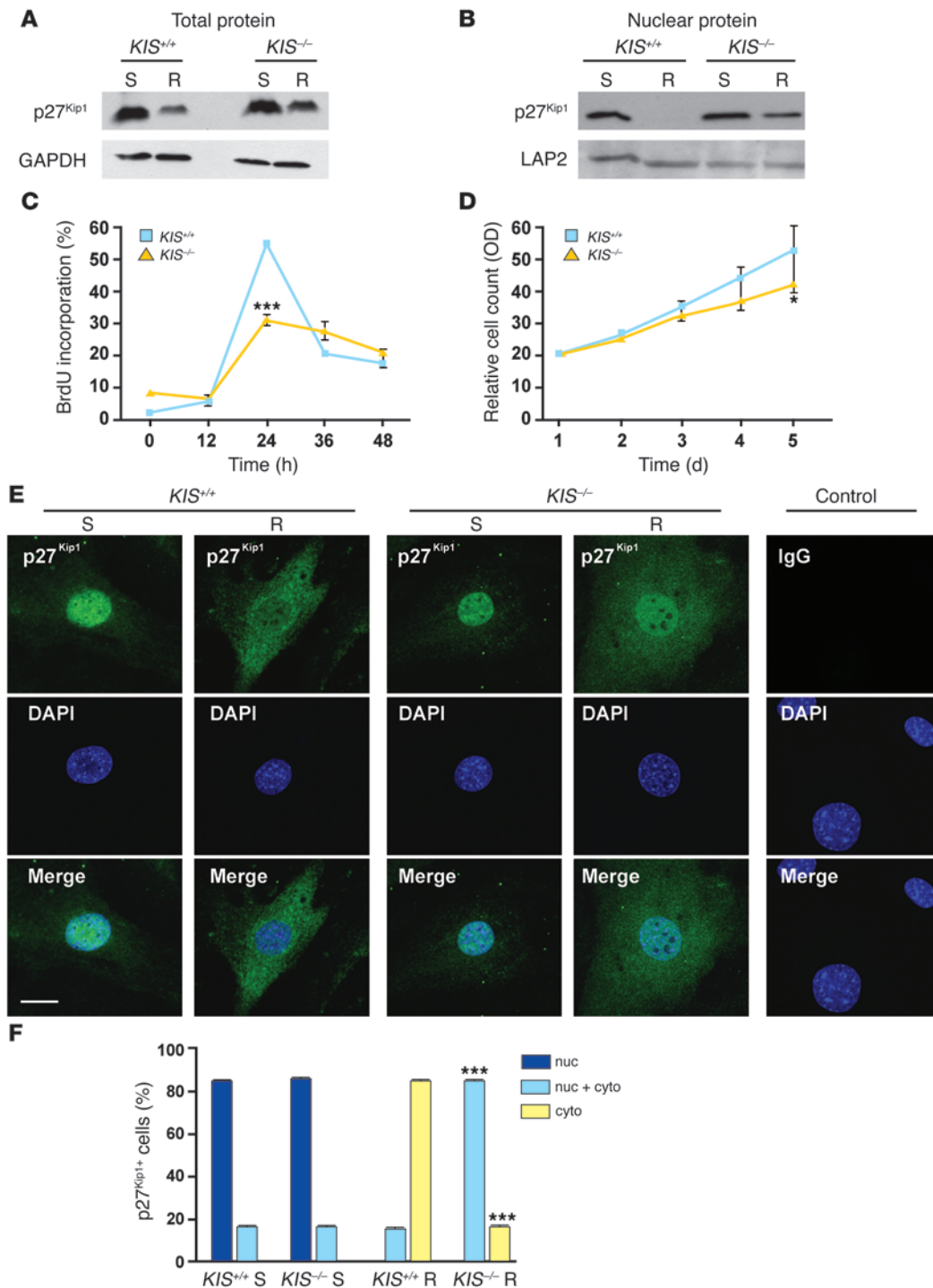
**Figure 5**
Delayed cell cycle progression in *KIS*^{−/−} VSMCs. (**A** and **B**) Western blot of p27[Kip1] using (**A**) total protein extracts of *KIS*^{+/+} and *KIS*^{−/−} VSMCs after serum starvation (S) and 12 hours after cell cycle release (R), and (**B**) nuclear protein extract of *KIS*^{+/+} and *KIS*^{−/−} VSMCs after serum starvation and 8 hours after cell cycle release. p27[Kip1] was completely exported from the nucleus in *KIS*^{+/+} VSMCs, whereas *KIS*^{−/−} VSMCs retained marked amounts of nuclear p27[Kip1]. GAPDH or LAP2 served as loading control. (**C**) *KIS*^{−/−} VSMCs showed a delayed entry into the S-phase (BrdU incorporation). *n* = 4. (**D**) *KIS*^{−/−} VSMCs proliferated slower than did *KIS*^{+/+} VSMCs. *n* = 9–15. (**E**) p27[Kip1] localization in *KIS*^{+/+} and *KIS*^{−/−} VSMCs after serum starvation and 8 hours after cell cycle release. After cell cycle release, most of the p27[Kip1] located to the nucleus and cytoplasm of *KIS*^{−/−} VSMCs, whereas most of the p27[Kip1] was exported into the cytoplasm of *KIS*^{+/+} VSMCs. Rabbit IgG served as negative control. Scale bar: 20 μm. (**F**) Quantification of p27[Kip1] immunostaining in the nucleus (nuc), cytoplasm (cyto), and nucleus and cytoplasm (nuc+cyto). *n* = 6. *$P < 0.05$, ***$P < 0.001$ vs. *KIS*^{+/+}.
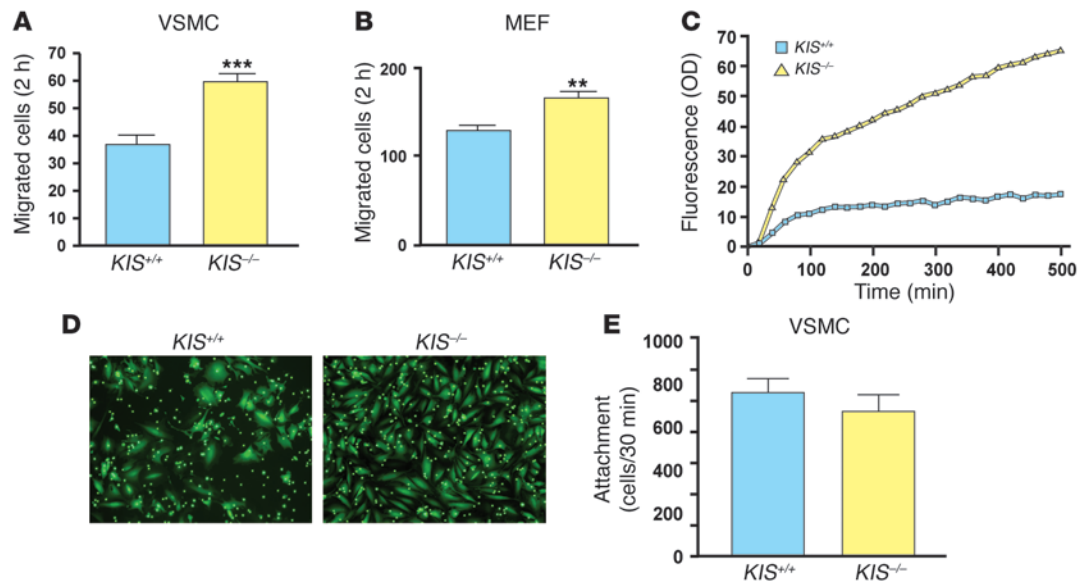
**Figure 6**
Increased migratory activity of *KIS*^{-/-} VSMCs and MEFs. (**A** and **B**) *KIS*^{-/-} VSMCs (**A**) and MEFs (**B**) migrated faster through 8-μm pores toward FBS and PDGF-BB within 2 hours than did *KIS*^{+/+} VSMCs and MEFs. *n* = 6 per group. (**C**) Increased migratory activity of *KIS*^{-/-} VSMCs in a time course experiment, in which fluorescent-labeled cells migrated through 3-μm pores toward FBS and PDGF-BB over 8 hours. Fluorescence was measured in the bottom chamber of the assay, corresponding to the number of migrated cells, and normalized to the total number of cells plated into the top chamber. (**D**) Fluorescent-labeled migrated cells in the bottom chamber were imaged at the end of the time course experiment, demonstrating a higher number of migrated *KIS*^{-/-} VSMCs. Original magnification, ×200. (**E**) Attachment of VSMCs to fibronectin was not different between the genotypes (*P* = NS). *n* = 6. **P* < 0.01, ***P* < 0.001 vs. *KIS*^{+/+}.

fected HEK293 cells with KIS and stathmin and measured stathmin protein concentrations by Western blot at 0, 3, and 6 hours after blocking protein synthesis with cycloheximide. Whereas stathmin protein abundance was greatly reduced over 6 hours, with an estimated half-life of approximately 2 hours, neither stathmin cotransfected with the kinase-deficient KIS mutant K54R nor S38A or S25/38A phosphorylation site mutants cotransfected with KIS were degraded (Figure 8D). These data suggest that KIS phosphorylates stathmin at serine 38 in vitro and in vivo and that this phosphorylation leads to degradation of stathmin. Phosphorylation of stathmin by KIS and subsequent degradation during $G_1$/S phase of the cell cycle might be relevant to reduce cell migration and prepare cells for mitosis.

*Deletion of KIS leads to cytoskeletal and focal adhesion rearrangements.* Changes in stathmin protein abundance is not necessarily accompanied by increased biological activity of the protein. To establish a link between increased stathmin protein concentration and cell motility, we investigated the arrangement of cytoskeletal proteins and the focal adhesion molecule vinculin. VSMCs were serum starved for 72 hours, plated onto fibronectin-coated cover slides in the presence of serum, allowed to attach for 8 hours, and stained for F-actin and acetylated tubulin. F-actin fibers rearranged toward the edges of *KIS*^{-/-} VSMCs, in contrast to the even cytoplasmic distribution pattern of F-actin fibers in *KIS*^{+/+} VSMCs (Figure 9A). Tubulin is present in 2 fractions: unmodified tubulin, with a short half-life, and modified tubulin, mostly acetylated, with a longer half-life. Increased acetylated tubulin correlates to reduced tubulin turnover and lower migratory activity of the cell (16). We also observed a higher abundance of stabilized acetylated tubulin in *KIS*^{+/+} versus *KIS*^{-/-} VSMCs (Figure 9A), suggestive of increased

tubulin-destabilizing activity and tubulin turnover in *KIS*^{-/-} cells. These findings were further supported by observations in a tubulin depolymerization assay. Tubulin polymerization was induced in vitro by adding taxol, a polymerization-inducing compound, to purified bovine tubulin. Polymerization was measured as incorporation of a fluorochrome into the forming microtubules. Taxol-induced polymerization was inhibited by addition of cell lysates from *KIS*^{+/+} VSMCs and was further significantly reduced by cell lysates from *KIS*^{-/-} VSMCs (Figure 9B).

Directed migration involves rearrangement of focal adhesion molecules such as vinculin toward the direction of migration. To test the ability of VSMCs to rearrange vinculin, a scratch wound assay was applied. VSMCs were grown on fibronectin-coated chamber slides to a semiconfluent layer and harvested 1 hour after application of a scratch wound. Vinculin staining revealed rearrangement of vinculin toward the direction of migration in *KIS*^{-/-} VSMCs (Figure 9A), whereas this rearrangement was not present in *KIS*^{+/+} VSMCs. These data demonstrate that *KIS*^{-/-} VSMCs display a higher tubulin destabilizing activity along with a higher rate of vinculin rearrangement upon initiation of migration, and support the phenotypic observation of higher migratory activity of *KIS*^{-/-} VSMCs.

*Knockdown of stathmin rescues the promigratory phenotype of KIS*^{-/-} *VSMCs.* To confirm that the observed phenotype is based on stathmin and to exclude the possibility that other tubulin-destabilizing proteins mediate the increased migration of *KIS*^{-/-} VSMCs, we performed a rescue experiment. Stathmin was downregulated by siRNA-mediated inhibition of transcription. The efficiency of stathmin-directed siRNA was verified by Western blot, which showed a dramatic reduction of stathmin expression using 3 different stathmin siRNAs (Figure 10A). No siRNA and scrambled
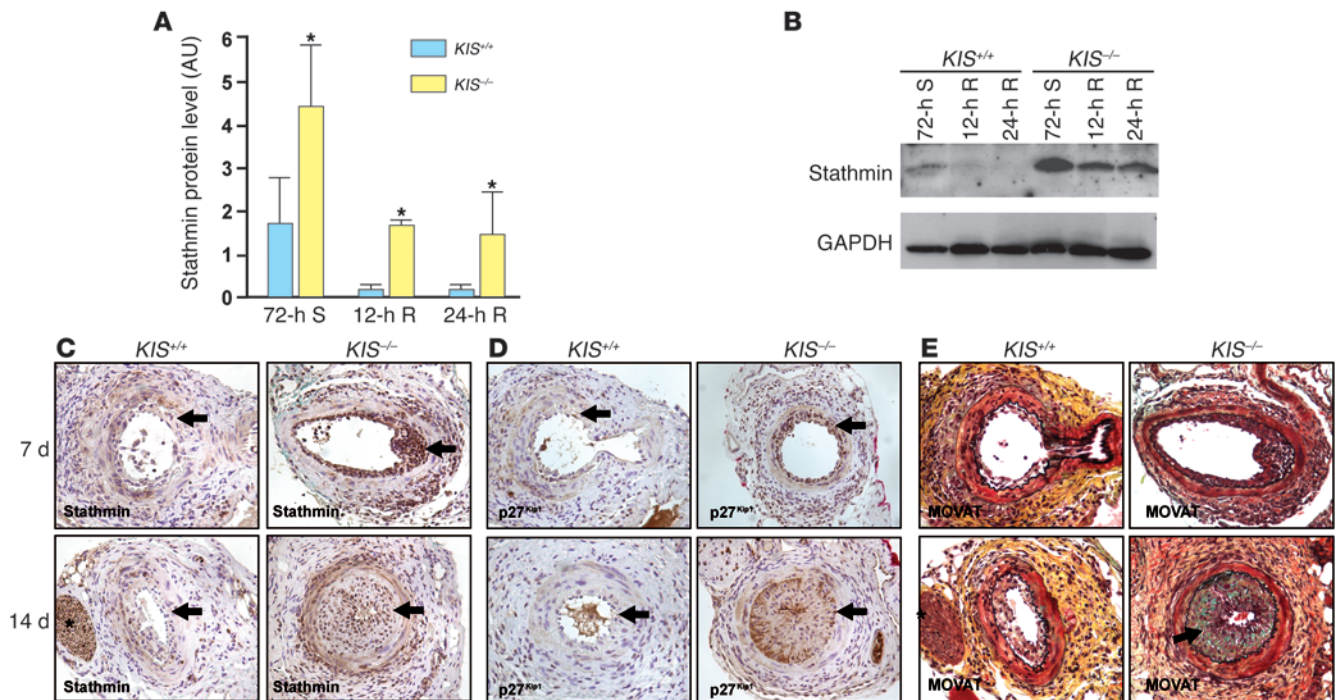
**Figure 7**
Increased stathmin expression in *KIS*⁻/⁻ VSMCs. (**A**) Quantitative analysis of 4 independent Western blots demonstrated increased cytoplasmic stathmin protein concentrations normalized to GAPDH in *KIS*⁻/⁻ VSMCs serum starved and released for the indicated times. *n* = 4. (**B**) Representative Western blot of stathmin expression in *KIS*⁺/⁺ and *KIS*⁻/⁻ VSMCs corresponding to quantitative data in **A**. GAPDH served as loading control. (**C** and **D**) Stathmin (**C**) and p27^Kip1 (**D**) immunohistochemistry demonstrated a higher abundance of stathmin and p27^Kip1 7 and 14 days after vascular injury in vessels of *KIS*⁻/⁻ mice than in *KIS*⁺/⁺ mice. Arrows denote internal elastica. (**E**) Movat pentachrome staining revealed increased accumulation of glycosaminoglycans 14 days after injury in the neointima of *KIS*⁻/⁻ mice compared with *KIS*⁺/⁺ mice (arrow indicates green staining), whereas there was no difference in extracellular matrix accumulation or composition between the genotypes 7 days after injury. Original magnification, ×400. *$P < 0.05$ vs. *KIS*⁺/⁺.

siRNA served as controls. Based upon these results, we used the siRNA designated st(3) in subsequent migration experiments. Knockdown of stathmin caused a small reduction in *KIS*⁺/⁺ VSMC migration (Figure 10B) corresponding to low baseline stathmin protein levels in *KIS*⁺/⁺ VSMCs. In contrast, knockdown of stathmin led to a marked reduction in *KIS*⁻/⁻ VSMCs migration; the extent of the reduction matched migration levels of *KIS*⁺/⁺ controls (*P* = NS; Figure 10B). These data demonstrate that the promigratory phenotype of *KIS*⁻/⁻ VSMCs is reversible by knockdown of stathmin and suggest that the observed phenotype is in fact based on increased abundance of active stathmin in *KIS*⁻/⁻ VSMCs.

To investigate the role of stathmin in VSMC migration in vivo, we conducted vascular injury experiments in *Stmn1*⁻/⁻ mice. We observed a significant reduction in neointima formation in *Stmn1*⁻/⁻ arteries compared with arteries from *Stmn1*⁺/⁺ littermates 14 days after vascular injury (intima/media area ratio, *Stmn1*⁺/⁺ 1.02 ± 0.12; *Stmn1*⁻/⁻ 0.60 ± 0.13, *P* < 0.05; Figure 10, C and D). These data suggest that stathmin promotes adverse vascular remodeling, because *Stmn1*⁻/⁻ mice are protected from lesion formation in response to vascular injury. The higher intima/media area ratio in *Stmn1*⁺/⁺ mice (Figure 10, C and D) compared with *KIS*⁺/⁺ mice (Figure 2, A and B) might be explained by the different genetic background of the mouse lines (C57BL6 and C57BL6/SV129, respectively) and emphasizes the importance of using littermates with the same genetic background as controls.

## Discussion

Vascular wound repair in response to mechanical arterial injury involves proliferation and migration of inflammatory and VSMCs. The complex mechanisms involved in this process are not fully understood. Here we provide genetic evidence for what we believe to be a novel mechanism regulating migration of VSMCs during vascular wound repair by KIS-dependent phosphorylation and degradation of stathmin. Ablation of KIS led to excessive neointima formation in a mouse model of mechanical arterial injury. *KIS*⁻/⁻ VSMCs displayed increased stathmin levels based on reduced phosphorylation by KIS and thus reduced degradation of stathmin, leading to increased microtubule turnover and augmented migration. Downregulation of stathmin reversed the promigratory phenotype of *KIS*⁻/⁻ VSMCs, further supporting the contribution of stathmin — as a KIS target protein — to neointima formation in this genetic model.

Stathmin has been proposed to regulate cell migration by promoting turnover of microtubules required for this cellular process (16, 17, 20, 21). The interaction between KIS and stathmin was first described by Maucuer et al. in a yeast 2-hybrid screen (2). The same group later reported KIS phosphorylation of stathmin on at least 1 serine residue; however, they concluded, by comparing stathmin phospho-peptide maps, that the KIS phosphorylation site was different from all known serine phosphorylation sites (4). This is contrary to our finding of KIS phosphorylation of stath-
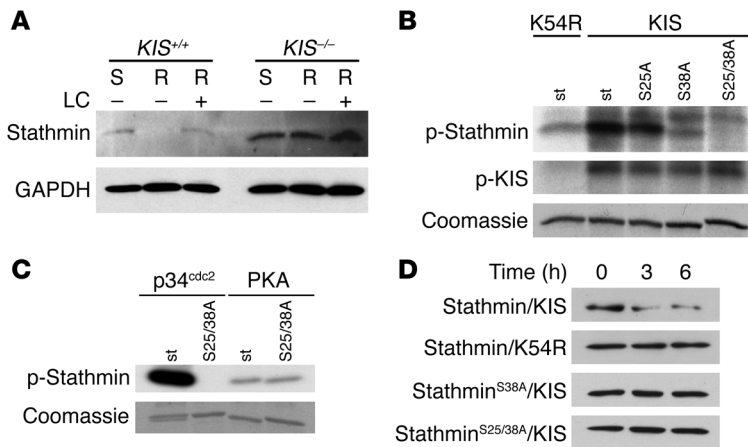
**Figure 8**
Stathmin degradation is determined by KIS-mediated phosphorylation of stathmin at serine 38. (**A**) VSMCs were serum starved for 72 hours or released for 12 hours, with or without treatment with the proteasome inhibitor LC. Cell cycle–dependent degradation of stathmin in $KIS^{+/+}$ VSMCs was inhibited by LC treatment and matched the stathmin level in serum-starved $KIS^{+/+}$ VSMCs, as measured by Western blot in the cytoplasmic protein fraction. LC treatment had little or no effect on stathmin protein expression in $KIS^{-/-}$ VSMCs. GAPDH served as loading control. (**B**) Kinase assays using KIS or the kinase-deficient mutant K54R as kinases and recombinant stathmin (st) or phosphorylation site mutants of stathmin as substrates. KIS phosphorylated stathmin and stathmin$^{S25A}$ (p-Stathmin). Phosphorylation of stathmin$^{S38A}$ and stathmin$^{S25/38A}$ was highly reduced or not detectable, which suggests that KIS phosphorylates stathmin at serine 38. Autophosphorylation of KIS (p-KIS) demonstrated equal KIS activity and effective reduction of kinase activity of K54R. Coomassie staining demonstrated equal loading. (**C**) Control experiment demonstrating that p34$^{cdc2}$ phosphorylated stathmin, but not stathmin$^{S25/38A}$, whereas PKA phosphorylated both substrates. (**D**) Half-life of stathmin was measured after coexpression of stathmin or stathmin phosphorylation site mutants along with KIS or K54R in HEK293 cells, followed by cycloheximide treatment.

min serine 38, which is 1 of the 4 known stathmin phosphorylation sites. Our finding might be explained by differences in experimental settings. Whereas Maucuer et al. generated recombinant GST-KIS in bacteria (4), which was very difficult to solubilize from inclusion bodies, we used overexpressed KIS without prior freezing for kinase assays. Moreover, we carried out the kinase assay in a different buffer, which we found led to higher activity of KIS toward stathmin. Our data were confirmed by using stathmin phosphorylation site mutants and further strengthened by overexpression experiments demonstrating a prolonged half-life of a stathmin S38A phosphorylation site mutant when coexpressed with KIS. Although KIS sustains dual serine and threonine kinase activity, Maucuer et al. recently reported that KIS preferentially targets proline-directed serine residues (5). This observation and the fact that stathmin carries only 2 serines within an SP motif at positions 25 and 38 further support our experimental findings.

A lack of stathmin phosphorylation in $KIS^{-/-}$ mice led to an accumulation of active stathmin in VSMCs, accounting for increased VSMC migration and excessive neointima formation after vascular injury. This was evident by the increased presence of luminal VSMCs in $KIS^{-/-}$ mice very early after vascular injury, abundant VSMCs within the neointima at later time points after injury, exclusion of increased cell proliferation in vivo and in vitro, rescue of the promigratory phenotype by siRNA-mediated down-regulation of stathmin in $KIS^{-/-}$ VSMCs in vitro, and reduced

neointima formation in $Stmn1^{-/-}$ mice in vivo. The difference in stathmin abundance was most pronounced in resting cells; however, upon mitogenic stimulation (early $G_1/S$ phase) and activation of KIS (3), stathmin was degraded in $KIS^{+/+}$ VSMCs. This degradation was diminished in $KIS^{-/-}$ VSMCs, leaving these cells with higher remaining active stathmin levels. Our findings relate, for the first time to our knowledge, stathmin function to cell migration in VSMCs in vitro and in vivo, demonstrate that VSMC migration is an important component of pathological wound repair, and suggest that VSMC migration is an excellent target for therapeutic intervention. Paclitaxel, a member of the taxane family of antitumor drugs, stabilizes microtubules and has previously been shown to effectively reduce restenosis when applied via drug-eluting stents (22–26). In this context, stathmin inhibition may be an interesting approach to specifically prevent VSMC migration, as stathmin is not dysregulated in $KIS^{-/-}$ T cells (our unpublished observations). $KIS^{+/+}$ and $KIS^{-/-}$ T cells displayed high migratory activity and showed high expression of stathmin regardless of their genotype, which suggests that the observed phenotype in this genetic model was caused by a VSMC phenotype. Additional evidence comes from abundant stathmin immunoreactivity in media and neointima of $KIS^{-/-}$ mice and the finding that ablation of T and B cells by cross-breeding $KIS^{-/-}$ mice with $Rag^{-/-}$ mice did not reduce neointima formation.

KIS is also linked to vascular proliferation by its interaction with the CDK inhibitor p27$^{Kip1}$. Experiments addressing cell cycle progression of VSMCs demonstrated, in accordance with our hypothesis, that KIS deletion results in delayed p27$^{Kip1}$ nuclear export and protein degradation and reduced proliferation of $KIS^{-/-}$ VSMCs, providing indirect evidence that migration is a predominant mechanism for vascular remodeling. Given that the cell cycle is only susceptible to mitogenic stimuli at $G_1/S$ and therefore tightly controlled, it is likely that there is redundancy in kinases targeting CDK inhibitors. In fact, at least 2 other kinases phosphorylate p27$^{Kip1}$ at serine 10, Myrk/Dyrk1b and CDK5 (27, 28). Evolving knowledge of p27$^{Kip1}$ phosphorylation by multiple kinases during different phases of the cell cycle, including the recent discovery that tyrosine phosphorylation by nonreceptor tyrosine kinases decreases p27$^{Kip1}$ stability and initiates cell cycle entry (29, 30), suggests a complex network of redundant kinases ensuring controlled p27$^{Kip1}$ degradation and cell cycle progression in vivo. Genetic mouse models carrying phosphorylation site mutants of p27$^{Kip1}$ offer a promising experimental approach to understanding the biology of p27$^{Kip1}$ phosphorylation during vascular wound repair.

In summary, our findings implicate a critical role of KIS during vascular wound repair by preventing excessive VSMC migration into the vascular lesion and further indicate that cell migration constitutes an important component of pathological vascular remodeling. Therapeutic disruption of vascular signaling that leads to uncontrolled migration through KIS activation and stathmin inhibition may benefit the treatment of vascular diseases, such as restenosis after coronary stent implantation or pulmonary hypertension.
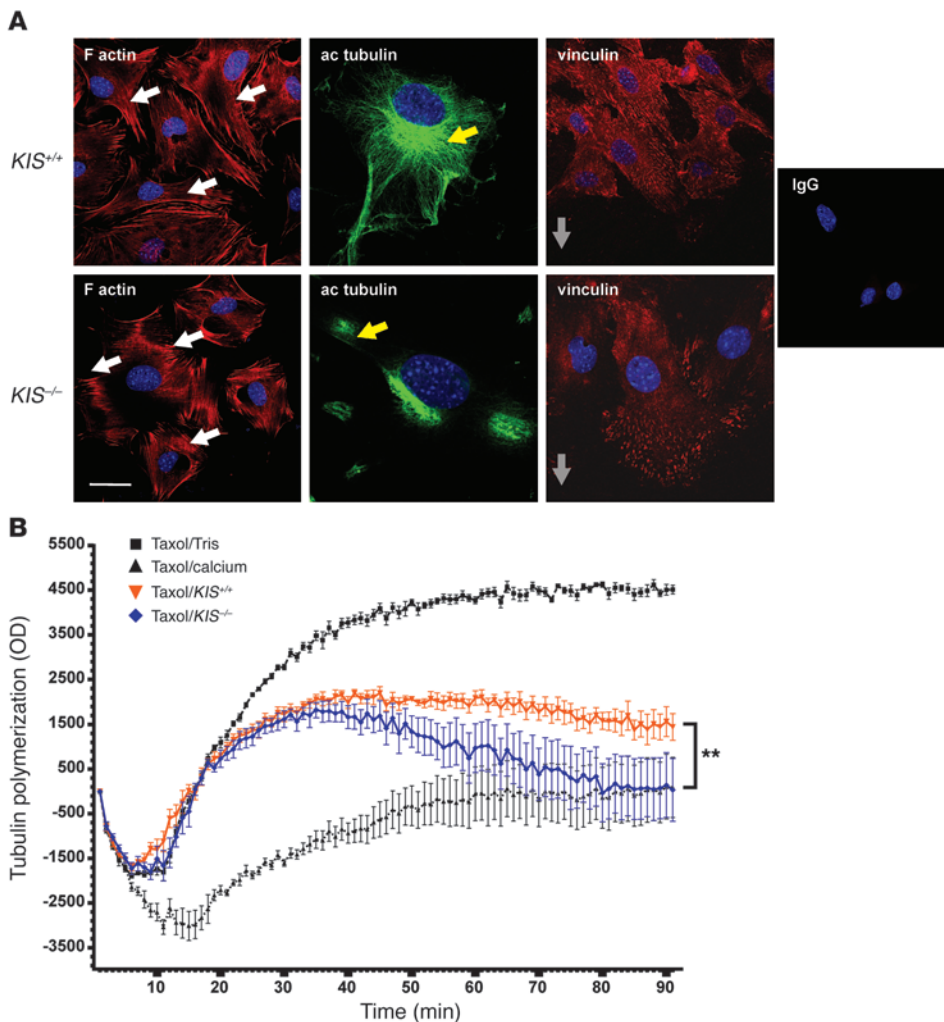
**Figure 9**
Rearrangement of cytoskeletal proteins and focal adhesions in $KIS^{-/-}$ VSMCs. (**A**) F-actin staining showed rearrangement of actin fibers (white arrows) away from the nucleus and toward the plasma membrane in $KIS^{-/-}$ VSMCs compared with $KIS^{+/+}$ VSMCs. Immunostaining for acetylated (ac) tubulin (yellow arrows) was reduced in $KIS^{-/-}$ compared with $KIS^{+/+}$ VSMCs. Vinculin was rearranged toward the direction of migration (gray arrows) within 1 hour in $KIS^{-/-}$ VSMCs in a wound scratch assay, whereas most $KIS^{+/+}$ VSMCs did not show rearrangement at that time point. IgG served as staining control. Scale bar: 20 μm. (**B**) Tubulin polymerization assay. Polymerization of recombinant tubulin was induced by taxol and measured as incorporation of a fluorescent dye into the tubulin fibers over time. $CaCl_2$ (calcium) and Tris-HCl served as controls. Addition of protein isolated from $KIS^{+/+}$ VSMCs partially inhibited tubulin formation, whereas the inhibition induced by protein isolated from $KIS^{-/-}$ VSMCs was complete, and the equilibrium was indistinguishable from that of the negative control at 90 minutes. $n = 4$. **$P < 0.01$, $KIS^{+/+}$ vs. $KIS^{-/-}$.

## Methods

*Gene targeting and generation of KIS$^{-/-}$ mice.* Regions of the mouse gene encoding KIS were cloned from mouse genomic DNA. The 5′ homology region of the targeting vector constituted a 1.9-kb KpnI-XhoI fragment of the KIS promoter, and the 3′ homology region was a 4.9-kb SalI-NotI fragment including exons 2 to 4 and respective introns. Both fragments were cloned into the targeting vector, leading to replacement of exon 1 with a neomycin resistance gene upon recombination. We electroporated 129SV mouse embryonic stem cells with the targeting vector, and recombined clones were identified by Southern blot. Further genotyping was carried out by PCR using primers KIS-WT-5P (5′-CCCGAGTTCAGTTCCCAGTG-3′), KIS-Neo-5P (5′-CCTAAGCTTGGCTGGACGTA-3′), and KIS-WT-3P (5′-TTCAGGCCTTTTGGCTGCCT-3′). Chimeric mice carrying the recombined allele were bred with C57BL6 mice. F1 heterozygous mice were intercrossed to yield $KIS^{-/-}$ and $KIS^{+/+}$ mice. All experiments were approved by and conducted according to the guidelines of the Animal Care and Use Committee of the National Heart, Lung, and Blood Institute (NHLBI).

*Vascular injury in mice.* Vascular wire injury of the femoral artery was performed as described previously (1). Tissues were harvested at 1, 3, 5, 7, and 14 days after injury. BrdU (25 mg/kg) was injected 24 hours and 1 hour before tissue harvest. Cross-sectional areas of intima and media were measured on H&E-stained sections by a single investigator blinded to genotype using Image-Pro Plus 5 software (Media Cybernetics). *Rag$^{-/-}$*

mice were purchased from Jackson Laboratories and crossbred with $KIS^{-/-}$ mice to obtain $KIS^{+/-}Rag^{+/-}$ mice. F1 heterozygous mice were intercrossed to obtain $KIS^{-/-}Rag^{+/+}$ and $KIS^{-/-}Rag^{-/-}$ mice. *Stmn1$^{-/-}$* mice, backcrossed to C57BL6 mice for 12 generations, were a gift from G. Shumyatsky (Rutgers University, Piscataway, New Jersey, USA).

*Cell culture.* Primary VSMCs were isolated from aortas of 5 mice of each genotype. Briefly, thoracic aortas were removed and rinsed in PBS. The media was carefully dissected from intima and adventitia under a stereo microscope, cut into small pieces, incubated with collagenase (1 mg/ml) and elastase (0.1 mg/ml) for 15 minutes at 37°C, and placed onto a 3.5-cm cell culture dish in 1 ml DMEM supplemented with 10% FBS, 100 U/ml penicillin, and 100 μg/ml streptomycin. Explants were incubated at 37°C for 7–10 days, and outgrown VSMCs were passaged by treatment with ×0.25 trypsin. Experiments were conducted on VSMCs at passage 5–8 that were serum starved by incubation in DMEM supplemented with 0.1% FBS for 72 hours and released by adding FBS to a final concentration of 20%. HEK293 cells were cultured in DMEM supplemented with 10% FBS, 100 U/ml penicillin, and 100 μg/ml streptomycin.

*Preparation of plasmid DNA and cell transfections.* Full-length human (h) stathmin was amplified from a human cDNA library by PCR and cloned into the XhoI/XbaI site of pcDNA3.1/HIS (Invitrogen) and the BamHI/EcoRI site of pGEX-6P (Amersham Biosciences). The phosphorylation site mutations S25A, S38A, and S25/38A were introduced into each stathmin-encoding plasmid using QuikChange Site Directed Mutagenesis Kit (Stratagene).
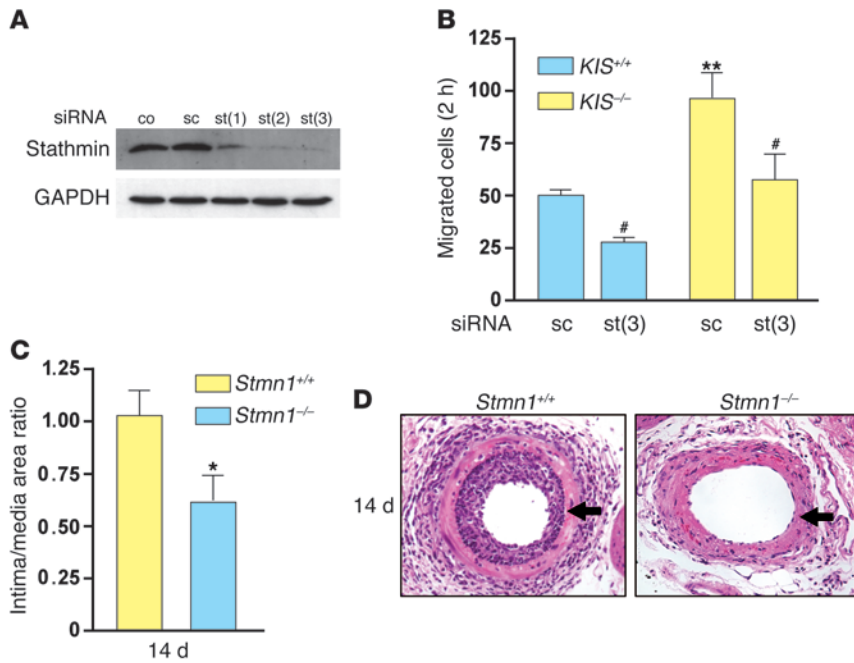
**Figure 10**
Rescue of the promigratory phenotype of *KIS*−/− VSMCs by siRNA-mediated downregulation of stathmin expression in vitro and in *Stmn1*−/− mice in vivo. (**A**) The delivery of 3 different stathmin-directed siRNAs [st(1)–st(3)] dramatically reduced stathmin protein concentrations as measured by Western blot; st(3) was the most efficient siRNA and was therefore used for subsequent experiments. No siRNA (co) and scrambled siRNA (sc) served as controls. GAPDH served as loading control. (**B**) siRNA-mediated downregulation of stathmin led to a reduction in migratory activity of *KIS*+/+ and *KIS*−/− VSMCs compared with scrambled siRNA controls. The migration of *KIS*−/− VSMCs after downregulation of stathmin matched the migration of scrambled siRNA–transfected *KIS*+/+ VSMCs (*P* = NS), suggesting a rescue of the promigratory phenotype of *KIS*−/− VSMCs by downregulation of stathmin. *n* = 6. (**C** and **D**) *Stmn1*−/− mice demonstrated less neointima formation 14 days after vascular injury than did *Stmn1*+/+ littermates, revealed by quantification of intima/media ratios (**C**) and representative H&E-stained sections (**D**; arrows denote internal elastica). *n* = 7–8 vessels per group. Original magnification, ×400. *$P < 0.05$ vs. *Stmn1*+/+; **$P < 0.01$ vs. *KIS*+/+ scrambled siRNA; #$P < 0.05$ vs. respective scrambled siRNA.

Generation of pcDNA3.1-(h)KIS, pcDNA3.1-(h)KIS(K54R), and pVR-1012p27Kip1 expression vectors was previously described (3). HEK293 cells were plasmid-DNA transfected using FuGENE 6 reagent (Roche). VSMCs were transfected with predesigned stathmin-directed or unspecific siRNA (Ambion) at a final concentration of 50 nM using Lipofectamine 2000 (Invitrogen) according to the manufacturer's protocol. Transfection efficiency was monitored with Cy3-labeled negative control siRNA (Ambion). Experiments were performed 3 days after siRNA transfection.

*Western blotting.* Cytoplasmic and nuclear protein fractions were isolated using the NE-PER kit (Pierce). For isolation of total cellular protein, cells were lysed in RIPA buffer for Western blotting or NP-40 buffer for immunoprecipitation, both supplemented with a protease inhibitor cocktail (Roche). Proteins were resolved on SDS-PAGE, blotted onto nitrocellulose membranes, and probed with a rabbit anti-stathmin antibody (1:20,000; Calbiochem), a rabbit anti-KIS antibody (1:250; Abgent), a mouse anti-GAPDH antibody (1:1,000; Abcam), a mouse anti-p27Kip1 antibody (1:1,000; BD Biosciences), or a goat anti-LAP2 antibody (1:200; Santa Cruz Biotechnology Inc.) as primary antibodies and anti-rabbit HRP (1:15,000; Santa Cruz Biotechnology Inc.), anti-goat HRP (1:10,000; Santa Cruz Biotechnology Inc.), or anti-mouse HRP (1:20,000; Amersham Biosciences) as secondary antibodies. Immunoreactivity was detected with SuperSignal West Pico or Femto Chemiluminescent

Substrates (Pierce). To analyze the degradation pattern of stathmin, VSMCs were treated with 10 μM LC to block proteasome-dependent protein degradation, starting 2 hours before release of the cells. For analysis of stathmin protein stability, 300 ng of pcDNA3.1-(h)stathmin or respective phosphorylation site mutants and 1.5 μg of pcDNA3.1-(h)KIS or the kinase-deficient KIS mutant pcDNA3.1-(h)KIS(K54R) were cotransfected into HEK293 cells. At 2 days after transfection, protein synthesis was inhibited by treatment with 100 μg/ml cycloheximide (Sigma-Aldrich), and overexpressed stathmin was measured by Western blotting using a rabbit anti-6x His tag antibody (1:1,000; Abcam).

*Immunostaining.* Immunohistochemistry on formalin-fixed and paraffin-embedded vascular sections was performed to detect SMA, BrdU, p27Kip1, CD3, F4/80, and neutrophils as described previously (1). Immunostaining of stathmin was conducted using a rabbit anti-stathmin antibody (1:50; Cell Signaling Technology). Immunofluorescence was performed on 4% paraformaldehyde-fixed VSMCs using a rabbit anti–p27Kip1C-19 antibody (1:50; Santa Cruz Biotechnology Inc.), rhodamine phalloidin (1 U/200 μl; Invitrogen), a mouse anti–acetylated α-tubulin antibody (1:500; Invitrogen), a mouse anti-vinculin antibody (1:50; Sigma-Aldrich), and goat anti-rabbit or goat anti-mouse Alex Fluor 488– or Alexa Fluor 568–conjugated secondary antibodies (1:1,000; Invitrogen). Cells were mounted in DAPI-containing medium (Vector Laboratories) and imaged with a Zeiss LMS510 confocal microscope. Movat pentachrome staining was performed to evaluate accumulation of glycosaminoglycans, as described previously (31). In this staining, elastic fibers stain black, collagen stains yellow, and glycosaminoglycans stain green.

*Migration studies.* MEFs or VSMCs were serum starved for 72 hours and plated into transwells with 8-μm pores (50,000 cells/well). Cells migrated toward fibronectin and DMEM supplemented with 20% FBS and mouse recombinant PDGF-BB (VSMCs only, 50 ng/ml; Biosource International). After 2 hours, cell migration was stopped by washing and fixation. The remaining cells were removed from the transwell using a cotton swab, and migrated cells were stained with DAPI and counted under a fluorescence microscope. We counted 5 representative fields of view per transwell, and the mean of migrated cells per field of view was calculated for each transwell. Data were calculated from 6 independent experiments. To assess the time course of migration, VSMCs were labeled with 10 μM Cell Tracker Green (Invitrogen) for 30 min at 37°C, and then plated into the top chamber of transwells with 3-μm pores (10,000 cells/well) and a FluoroBlock membrane (BD Biosciences). Fluorescence in the bottom chamber was measured as a function of time in a plate reader (Tecan) at 37°C, representing the total number of migrated cells and normalized to the total fluorescence in the transwell at the beginning of the experiment.

*Tubulin polymerization assay.* Total protein of serum-starved VSMCs was retrieved by 3 freezing and thawing cycles in 30 mM Tris-HCl (pH 7.5). The protein was concentrated to 10 μg/μl using Microcon Centrifugal Filter Devices (Millipore). Tubulin polymerization was measured using a Tubulin Polymerization Assay Kit (Cytoskeleton). Taxol served as positive control.

Protein (50 μg) from *KIS*^{-/-} or *KIS*^{+/+} VSMCs was added to taxol to measure the activity of microtubule-destabilizing factors in the cell lysate. Tris-HCl (pH 7.5) and CaCl$_2$ (30 mM each) served as negative controls. Data were calculated from 4 independent experiments.

*Statistics*. Statistical data analysis was performed by ANOVA followed by Bonferroni multiple-comparison correction or by unpaired 2-tailed Student's *t* test as appropriate. Results are presented as mean ± SEM. A *P* value less than 0.05 was considered significant.

1. Boehm, M., et al. 2004. Bone marrow-derived immune cells regulate vascular disease through a p27(Kip1)-dependent mechanism. *J. Clin. Invest.* **114**:419–426.
2. Maucuer, A., Camonis, J.H., and Sobel, A. 1995. Stathmin interaction with a putative kinase and coiled-coil-forming protein domains. *Proc. Natl. Acad. Sci. U. S. A.* **92**:3100–3104.
3. Boehm, M., et al. 2002. A growth factor-dependent nuclear kinase phosphorylates p27(Kip1) and regulates cell cycle progression. *EMBO J.* **21**:3390–3401.
4. Maucuer, A., et al. 1997. KIS is a protein kinase with an RNA recognition motif. *J. Biol. Chem.* **272**:23151–23156.
5. Maucuer, A., Le Caer, J.P., Manceau, V., and Sobel, A. 2000. Specific Ser-Pro phosphorylation by the RNA-recognition motif containing kinase KIS. *Eur. J. Biochem.* **267**:4456–4464.
6. Polyak, K., et al. 1994. Cloning of p27Kip1, a cyclin-dependent kinase inhibitor and a potential mediator of extracellular antimitogenic signals. *Cell.* **78**:59–66.
7. Sherr, C.J., and Roberts, J.M. 1999. CDK inhibitors: positive and negative regulators of G1-phase progression. *Genes Dev.* **13**:1501–1512.
8. Belmont, L.D., and Mitchison, T.J. 1996. Identification of a protein that interacts with tubulin dimers and increases the catastrophe rate of microtubules. *Cell.* **84**:623–631.
9. Howell, B., Larsson, N., Gullberg, M., and Cassimeris, L. 1999. Dissociation of the tubulin-sequestering and microtubule catastrophe-promoting activities of oncoprotein 18/stathmin. *Mol. Biol. Cell.* **10**:105–118.
10. Labdon, J.E., Nieves, E., and Schubart, U.K. 1992. Analysis of phosphoprotein p19 by liquid chromatography/mass spectrometry. Identification of two proline-directed serine phosphorylation sites and a blocked amino terminus. *J. Biol. Chem.* **267**:3506–3513.
11. Beretta, L., Dobransky, T., and Sobel, A. 1993. Multiple phosphorylation of stathmin. Identification of four sites phosphorylated in intact cells and in vitro by cyclic AMP-dependent protein kinase and p34cdc2. *J. Biol. Chem.* **268**:20076–20084.
12. Di Paolo, G., Antonsson, B., Kassel, D., Riederer, B.M., and Grenningloh, G. 1997. Phosphorylation regulates the microtubule-destabilizing activity of stathmin and its interaction with tubulin. *FEBS Lett.* **416**:149–152.
13. Marklund, U., Osterman, O., Melander, H., Bergh, A., and Gullberg, M. 1994. The phenotype of a "Cdc2 kinase target site-deficient" mutant of oncoprotein 18 reveals a role of this protein in cell cycle control. *J. Biol. Chem.* **269**:30626–30635.
14. Brattsand, G., Marklund, U., Nylander, K., Roos, G., and Gullberg, M. 1994. Cell-cycle-regulated phosphorylation of oncoprotein 18 on Ser16, Ser25 and Ser38. *Eur. J. Biochem.* **220**:359–368.
15. Larsson, N., Melander, H., Marklund, U., Osterman, O., and Gullberg, M. 1995. G2/M transition requires multisite phosphorylation of oncoprotein 18 by two distinct protein kinase systems. *J. Biol. Chem.* **270**:14175–14183.
16. Baldassarre, G., et al. 2005. p27(Kip1)-stathmin interaction influences sarcoma cell migration and invasion. *Cancer Cell.* **7**:51–63.
17. Jin, K., et al. 2004. Proteomic and immunochemical characterization of a role for stathmin in adult neurogenesis. *FASEB J.* **18**:287–299.
18. Liedtke, W., Leman, E.E., Fyffe, R.E., Raine, C.S., and Schubart, U.K. 2002. Stathmin-deficient mice develop an age-dependent axonopathy of the central and peripheral nervous systems. *Am. J. Pathol.* **160**:469–480.
19. Shumyatsky, G.P., et al. 2005. Stathmin, a gene enriched in the amygdala, controls both learned and innate fear. *Cell.* **123**:697–709.
20. Giampietro, C., et al. 2005. Stathmin expression modulates migratory properties of GN-11 neurons in vitro. *Endocrinology.* **146**:1825–1834.
21. Ng, D.C., et al. 2006. Stat3 regulates microtubules by antagonizing the depolymerization activity of stathmin. *J. Cell Biol.* **172**:245–257.
22. Grube, E., et al. 2005. Two-year-plus follow-up of a paclitaxel-eluting stent in de novo coronary narrowings (TAXUS I). *Am. J. Cardiol.* **96**:79–82.
23. Grube, E., et al. 2003. TAXUS I: six- and twelve-month results from a randomized, double-blind trial on a slow-release paclitaxel-eluting stent for de novo coronary lesions. *Circulation.* **107**:38–42.
24. Tanabe, K., et al. 2003. TAXUS III Trial: in-stent restenosis treated with stent-based delivery of paclitaxel incorporated in a slow-release polymer formulation. *Circulation.* **107**:559–564.
25. Turco, M.A., et al. 2007. Polymer-based, paclitaxel-eluting TAXUS Liberte stent in de novo lesions: the pivotal TAXUS ATLAS trial. *J. Am. Coll. Cardiol.* **49**:1676–1683.
26. Weissman, N.J., et al. 2005. Polymer-based paclitaxel-eluting stents reduce in-stent neointimal tissue proliferation: a serial volumetric intravascular ultrasound analysis from the TAXUS-IV trial. *J. Am. Coll. Cardiol.* **45**:1201–1205.
27. Deng, X., Mercer, S.E., Shah, S., Ewton, D.Z., and Friedman, E. 2004. The cyclin-dependent kinase inhibitor p27Kip1 is stabilized in G(0) by Mirk/dyrk1B kinase. *J. Biol. Chem.* **279**:22498–22504.
28. Kawauchi, T., Chihama, K., Nabeshima, Y., and Hoshino, M. 2006. Cdk5 phosphorylates and stabilizes p27kip1 contributing to actin organization and cortical neuronal migration. *Nat. Cell Biol.* **8**:17–26.
29. Grimmler, M., et al. 2007. Cdk-inhibitory activity and stability of p27Kip1 are directly regulated by oncogenic tyrosine kinases. *Cell.* **128**:269–280.
30. Chu, I., et al. 2007. p27 phosphorylation by Src regulates inhibition of cyclin E-Cdk2. *Cell.* **128**:281–294.
31. Farb, A., Weber, D.K., Kolodgie, F.D., Burke, A.P., and Virmani, R. 2002. Morphological predictors of restenosis after coronary stenting in humans. *Circulation.* **105**:2974–2980.